

FULL PAPER

Synthesis, XRD, spectral (IR, UV–Vis, NMR) characterization and quantum chemical exploration of benzoimidazole-based hydrazones: A synergistic experimental-computational analysis

Muhammad Rafiq¹ | Muhammad Khalid²  | Muhammad Nawaz Tahir³ |
Muhammad Umair Ahmad¹ | Muhammad Usman Khan⁴ |
Muhammad Moazzam Naseer⁵ | Atualpa Albert Carmo Braga⁶ |
Shabbir Muhammad⁷ | Zahid Shafiq¹

¹Institute of Chemical Sciences, Bahauddin Zakariya University, Multan 60800, Pakistan

²Department of Chemistry, Khwaja Fareed University of Engineering & Information Technology, Rahim Yar Khan-64200, Pakistan

³Department of Physics, University of Sargodha, Sargodha 40100, Pakistan

⁴Department of Applied Chemistry, Government College University, Faisalabad 38000, Pakistan

⁵Department of Chemistry, Quaid-i-Azam University, Islamabad 45320, Pakistan

⁶Departamento de Química Fundamental, Instituto de Química, Universidade de São Paulo, Avenida Professor Lineu Prestes, 748, São Paulo 05508-000, Brazil

⁷Department of Physics, College of Science, King Khalid University, Abha 61413P.O. Box 9004, Saudi Arabia

Correspondence

Muhammad Khalid and Zahid Shafiq, Department of Chemistry, Khwaja Fareed University of Engineering & Information Technology, Rahim Yar Khan-64200, Pakistan.

Email: khalid@iq.usp.br; muhammad.khalid@kfueit.edu.pk; zahidshafiq25@hotmail.com

Funding information

Brazilian National Research Council (CNPq), Grant/Award Number: AACB

Present study advocates the joint experimental and computational studies of two potent benzoimidazole-based hydrazones with chemical formula $C_{23}H_{18}F_2N_4O$ (**5a**) and $C_{25}H_{22}FN_5O_3$ (**5b**). Both **5a** and **5b** were synthesized and resolved into their crystal structures using SC-XRD for the assessment of bond lengths, bond angles, unit cells and space groups. The structures of **5a** and **5b** were chemically characterized using infrared (FT-IR), UV–Visible, nuclear magnetic resonance (¹H-NMR and ¹³C-NMR), EIMS and elemental analysis. DFT at M06-2X/6-31G(d,p) level of theory was performed to get optimized structures and countercheck the experimental findings. Overall, DFT findings show excellent concurrence with the experimental data which confirms the purity of both compounds. FMO, NBO analysis, MEP surfaces and nonlinear optical (NLO) properties were explored at same level of theory. UV–Vis analysis at TDDFT/M06-2X/6-31G(d,p) level of theory showed that **5b** is red shifted with λ_{max} 331.69 nm as compared to **5a** with λ_{max} 240.25 nm. Global reactivity parameters were estimated using energy of FMOs indicated the greater harness value than the softness values of **5a** and **5b**. NBO analysis confirmed that the presence of non-covalent interactions, hydrogen bonding and hyper conjugative interactions are pivotal cause for the existence of **5a** and **5b** in the solid-state. NLO results of **5a** and **5b** were observed better than standard molecule recommended the NLO activity of said molecules for optoelectronic applications.

Highlights

- Two novel benzoimidazole-based hydrazones were synthesized.
- XRD, NMR, FT-IR, UV-Vis, EIMS and elemental analysis were performed for the characterization.

(grant 309715/2017-2); Coordenação de Aperfeiçoamento de Pessoal de Nível Superior - Brasil (CAPES), Grant/Award Number: Finance Code 001; Deanship of Scientific Research at King Khalid University, Saudi Arabia, Grant/Award Number: grant number (R.G.P.2/45/40); Fundação de Amparo à Pesquisa do Estado de São Paulo, Grant/Award Numbers: 2015/01491-3, 2014/25770-6, grants # 2011/07895-8

- Computational study was done at M06-2X/6-31G(d,p) level for comparative study.
- Comparative study reveals a good agreement between experimental and DFT results.
- FMO, NLO and NBO analysis were performed.

KEYWORDS

Benzimidazole-based hydrazones, DFT, NLO, non-covalent interactions, spectroscopic data

1 | INTRODUCTION

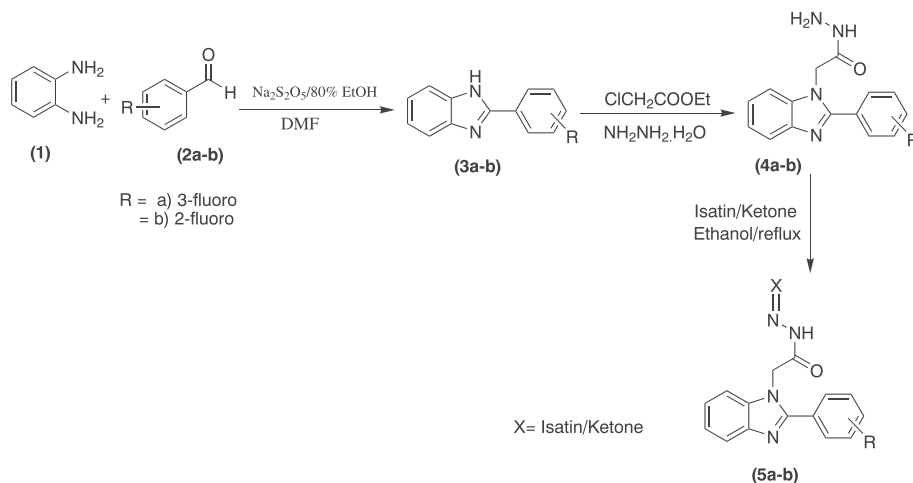
Benzimidazole derived compounds are class of N-comprising heterocyclic motifs widely used in organic and medicinal chemistry as imperative pharmacophore exhibiting various biological activities.^[1] These compounds are bicyclic in nature which consists of the fusion of benzene.^[2] Heterocyclic structures have been widely applied during the process of drug development.^[3] Benzimidazole is structurally similar to naturally occurring molecule purine that makes it a vital structural motif in drug design and simply interacts with biomolecules of the living systems.^[4] The rigid aromatic system that present in the structure of benzimidazole gives rise to specific spectroscopic which makes it an active probe for nucleic acids. Recently, benzimidazole and its derivatives have attained considerable attention due to their potential applications as antiulcer (omeprazole),^[5] tubulin polymerization inhibitor,^[6] anti-hypertensive,^[7] antifungal,^[8] anticancer,^[9] anthelmintic,^[10] antibacterial,^[11] cytotoxicity,^[12] antimicrobial,^[13] anti-inflammatory,^[14] antitumor,^[15] Trypanosomacruzi (Tc) infection,^[16] histamine-H3 antagonist, antioxidant, gastro protective and anti-parasitic, DNA binding and DNA-encoded library (DEL) technology,^[17,18] enzyme inhibition,^[19] Alzheimer disease (AD)^[20] and HIV-1 induced inhibitor for cytopathic activity. Furthermore, these derivatives have been employed as organic ligands,^[21] corrosion science,^[1] functional materials, catalysis,^[22,23] chemosensing, fluorescence signaling,^[24] self-aggregation^[25] and dye sensitized solar cells (DSSCs).^[26]

Hydrazones are well-documented in literature as framework of organic compounds with tremendous potential as target for various biological activities. Heterocycles derived from hydrazones have been described to show anticonvulsant and antiproliferative activities.^[27] Acyl hydrazones have been found to display significant biological activities such as antiplatelet, antibacterial, antimalarial, antituberculosis, antifungal, analgesic, anticancer and anticonvulsant activities.^[28] Currently, hydrazones and

benzimidazole derivatives have revealed excellent α -glucosidase inhibitory activity. To the best of our knowledge, there are hitherto very few reports of benzimidazole based hydrazones as α -glucosidase inhibitors.^[29]

Organic crystals are progressively been known as valuable materials with broad scope owing to their molecular nature. By tuning the structures along with the versatility provided by synthetic organic chemistry, the improved molecular structure can be explored with increased nonlinear properties.^[30–35] Organic crystals have been systematically examined^[36–44] due to their prompt reaction in electro-optic, high nonlinearities, and tailor made flexibility. Benzimidazole is one of the organic material and its single crystals possessing outstanding nonlinear optical properties.^[45,46] The imidazole unit is stable chemically and omnipresent in biological systems as well as remarkable backbone for compounds that demonstrate externally switchable polarization in crystalline conditions.^[47]

In present study, synthesis, single crystal X-ray diffraction (SC-XRD) and density functional theory (DFT) studies of two potent benzimidazole-based hydrazones: (E)-2-(2-(3-fluorophenyl)-1H-benzo[d]imidazol-1-yl)-N'-(1-(4-fluorophenyl)ethyl-iden)acetohydrazide (**5a**) and (Z)-2-(2-(2-fluorophenyl)-1H-benzo[d]imidazol-1-yl)-N'-(5-methyl-2-oxoindolin-3-ylidene) acetohydrazide (**5b**) have been reported for the first time (Scheme 1). The structures of **5a** and **5b** were characterized using spectroscopic FT-IR, UV-Visible, ¹H and ¹³C-NMR, EIMS and elemental analysis. The experimentally obtained spectroscopic and structural characteristics were further counterchecked by employing DFT. Moreover, DFT based calculations have been performed to estimate frontier molecular orbitals (FMO), natural bond orbital (NBO), global reactivity parameters, molecular electrostatic potential (MEP) surfaces and NLO properties. The ultimate goal of this study involves a precise and thorough account of experimental and theoretical data for clear understanding of structural and spectroscopic aspects of **5a** and **5b**.



SCHEME 1 Schematic representation for the synthesis of **5a** and **5b**

2 | MATERIALS AND METHODS

2.1 | Experimental section

The synthesis of target hydrazones (**5a-b**) was achieved through reaction sequence outlined in Scheme-1. *1H*-benzimidazoles (**3a-b**) were prepared by oxidative condensation of appropriate aldehyde (**2a-b**) with *o*-phenylenediamine and sodium metabisulfite.^[48] Compounds (**3a-b**) were reacted with ethyl bromoacetate in KOH/DMSO to furnish the *N*-substituted esters which on subsequent treatment with hydrazine hydrate under reflux in ethanol gave the respective hydrazides (**4a-b**). The hydrazides were then condensed with 4-fluoro acetophenone and 5-methylisatin in refluxing ethanol to afford the targeted hydrazones (**5a-b**) in excellent yields (81–85%).

The structures of new hydrazones were established on the basis of their microanalysis (CHN) and spectral data i. e. IR, ¹H NMR, ¹³C NMR and ESI. The NH band in IR appeared in the range of 3068–3197 cm⁻¹ while C=N stretching in the range of 1611–1623 which is in accordance with the formation of new azomethine C=N bond in hydrazones. In ¹H NMR of **5a**, the NH signal was observed at δ 11.08 ppm while a singlet appeared at δ 2.28 ppm for CH₃ group. A deshielded singlet for two protons of N-CH₂-CO appeared at δ 5.59 ppm due to the presence of electron withdrawing CO group. The aromatic protons of benzimidazole ring appeared as multiplet in the range from δ 7.21–7.29 while the aromatic protons of other two rings were deshielded due to the presence of F atoms and observed in the range of δ 7.46–7.92 ppm. In ¹H NMR of **5b**, a broad singlet for isatin NH appeared at δ 12.64 ppm while NH of hydrazone functionality appeared at δ 11.18 ppm. N-CH₂-CO proton was found at δ 5.53 ppm and CH₃ at 5-

position of isatin ring appeared at N-CH₂-CO appeared at δ 2.27 ppm. The other signals assigned to aromatic protons and in ¹³C NMR also supported the structure of desired compounds. The mass spectrometry of the hydrazones (**5a-b**) confirmed the exact mass. Furthermore the structure was also confirmed by unambiguous characterization of the compound **5a-b** by X-ray single crystal analysis.

2.2 | General procedure for the synthesis of Hydrazones (3a-b)

Mixture of an appropriate aldehyde and Na₂S₂O₅ (2:1) were stirred in 20 ml of ethanol at room temperature for 30 min. More ethanol was added and allowed the reaction mixture to cool in ice bath for several hours. The precipitates of the adduct of benzaldehyde formed were filtered and dried. The mixture of equimolar salt (adduct of benzaldehyde) and *o*-phenylenediamine in DMF (40 ml) were refluxed at 130–150 °C for 5–12 hrs. After the completion of reaction as monitored by TLC, the reaction mixture was poured into ice cool water and the solid benzimidazole derivatives (**3a-b**) were filtered and dried under vacuum. In the next step, DMSO was added to potassium hydroxide (crushed pellets) (1:1) and the mixture was stirred for 15 mins. Benzimidazole was added and the resultant mixture was stirred for 2 hrs followed by the addition of ethylchloroacetate on cooling and stirring was continued for further 2 hrs. The reaction was quenched by the addition of water and the mixture was extracted with ether. The procedure was repeated 3 times and the combined organic layers were dried over anhydrous sodium sulphate. Evaporation of the solvent gave the desired benzimidazole esters which were used in the next step. To a hot stirred

solution of corresponding benzimidazole, ester was added equimolar quantity of hydrazine hydrate in ethanol (10 ml) and the resultant reaction mixture was refluxed for 15 min. After completion, the reaction mixture was cooled and poured into cold water. The crude product (benzimidazole hydrazide) was filtered off and dried. The products (**4a-b**) were purified by crystallization in ethanol. For hydrazone synthesis, benzimidazole hydrazide and appropriate carbonyl compounds (ketone/isatin) in ethanol (10 ml) was refluxed for several hours. The reaction was monitored by TLC. The crystalline solid formed during refluxing was collected by suction filtration. Thorough washing with hot methanol followed by ether afforded the desired compounds (**5a-b**) in pure form.

2.3 | Computational procedure

The overall quantum chemical calculations for compounds **5a** and **5b** were performed with the help of DFT^[49–51] employing Gaussian 09 program package.^[52] The global hybrid meta exchange-correlation functional M06-2X^[53] and the Pople style 6–31G(d,p) basis set was utilized for all calculations.^[54] Gas-phase geometry optimization without symmetry restrictions was done after elucidating the initial geometry of **5a** and **5b** from XRD driven crystal structures. The vibrational analysis at DFT/M06-2X/6-31G(d,p) functional were executed which provide positive frequencies in all calculations and proved that the investigated systems **5a** and **5b** are at local minima in potential energy surfaces. The natural bond orbital (NBO)^[55] analysis, frontier molecular orbital (FMO) analysis and molecular electrostatic potential (MEP) analysis were studied at same level of theory, whereas, the UV–Vis spectra was calculated by TDDFT/M06-2X/6-31G(d,p) level of theory. All the input files were prepared by Gauss View 5.0.^[56] Finally, the Avogadro,^[57] Gauss View 5.0 and Chemcraft^[58] programs were employed for interpreting output files.

3 | RESULTS AND DISCUSSION

Synthesis of E)-2-(2-(3-fluorophenyl)-1H-benzo[d]imidazol-1-yl)-N'-(1-(4-fluorophenyl)ethyl- idene)acetohydrazide (**5a**)

Color: Yellow solid; **Yield:** 85%, **m.p.** 235–236 °C; **IR** (KBR) ν (cm⁻¹): 3197 (NH), 1611 (C=N), 1672 (CONH), **¹H-NMR** (DMSO-*d*⁶) δ ppm; 2.28 (s, 3H, CH₃), 5.59 (s, 2H, N-CH₂-CO), 7.21–7.29 (m, 5H), 7.56–7.61 (m, 4H), 7.72–7.74 (m, 1H), 7.88–7.92 (m, 2H), 11.08 (bs, 1H, NH), **¹³C NMR** δ ppm; 14.28, 46.62, 111.35, 115.76,

116.31, 117.29, 119.63, 122.74, 123.36, 125.48, 129.12, 131.48, 134.83, 137.18, 142.66, 148.87, 152.72, 161.48, 162.33, 163.42, 164.29, 169.68; **Anal calcd** for C₂₃H₁₈F₂N₄O (404.14); C, 68.31; H, 4.49; N, 13.85; Found C, 68.36; H, 4.56; N, 13.83.

Synthesis of (Z)-2-(2-(2-fluorophenyl)-1H-benzo[d]imidazol-1-yl)-N'-(5-methyl-2-oxoindolin-3-ylidene)acetohydrazide (**5b**)

Color: Light orange solid; **Yield:** 81%, **m.p.** 204–205 °C; **IR** (KBR) ν (cm⁻¹): 3068 (NH), 1623 (C=N), 1690 (CONH), **¹H-NMR** (DMSO-*d*⁶) δ ppm; 2.27 (s, 3H, CH₃), 5.53 (s, 2H, N-CH₂-CO), 6.83 (d, 1H, *J* = 8.0 Hz), 7.18 (d, 1H, *J* = 7.6 Hz), 7.29–7.33 (m, 2H), 7.37–7.44 (m, 2H), 7.61–7.66 (m, 3H), 7.72–7.75 (m, 1H), 11.18 (bs, 1H, NH), 12.64 (bs, 1H, NH); **¹³C-NMR** δ ppm; 20.94, 45.29, 111.47, 111.67, 116.64, 116.81, 118.22, 118.34, 119.73, 121.74, 122.75, 123.44, 125.53, 132.23, 132.79, 132.83, 133.07, 133.14, 140.84, 143.07, 149.17, 159.05, 161.02, 163.03; **Anal calcd** for C₂₄H₁₈FN₅O₂ (427.14); C, 67.44; H, 4.24; N, 16.38; Found C, 67.46; H, 4.28; N, 16.31.

3.2 | Structural insight by SC-XRD study

The crystal data, data collection parameters and refinement results of **5a** and **5b** are summarized in Table 1.

Good quality single crystals of benzoimidazole-based hydrazones **5a** and **5b** were cultivated by the slow evaporation of their solutions (Table 1). Both compounds **5a** and **5b** crystallize in monoclinic systems having *P*₂₁/*n* and *P*₂₁/*c* space groups, respectively. It is also important to mention that compound **5b** crystallizes as methanol solvate. The molecular structures (ORTEP diagram) of benzoimidazole-based hydrazones **5a** and **5b** along with crystallographic numbering schemes are shown in Figure 1. The 4-fluorophenyl and 5-methylisatin moieties that are linked to the benzoimidazole through central acetohydrazone moiety in compound **5a** and **5b** respectively, are present nearly in the same plane as the central acetohydrazone moiety in their solid state structures [N(4)-N(3)-C(15)-O(1) -174.86(18), N(4)-N(3)-C(15)-C(14) 5.7(3), N(4)-C(16)-C(18)-C(23) -13.7(3)] in **5a** and [N(4)-N(3)-C(15)-O(1) 175.42(19), N(4)-N(3)-C(15)-C(14) -3.3(3), N(4)-C(16)-C(19)-C(18) -176.7(2) in **5b**]. This planarity can be attributed to the significant amount of delocalization of nitrogen lone pair of amide moieties to the carbonyl group in both **5a** and **5b**, leading to the extension of conjugation of 4-fluorophenyl- and 5-methylisatin-hydrazone moieties. This is clearly manifested by the partial double bond character of N-C bonds

TABLE 1 X-ray crystallographic data of **5a** and **5b**

Crystal data	5a	5b
CCDC	1911377	1911378
Chemical formula	C ₂₃ H ₁₈ F ₂ N ₄ O	C ₂₅ H ₂₂ FN ₅ O ₃
<i>M_r</i>	404.41	459.47
Crystal system, space group	Monoclinic, <i>P</i> ₂ ₁ / <i>n</i>	Monoclinic, <i>P</i> ₂ ₁ / <i>c</i>
Temperature (K)	296	296
<i>a</i> , <i>b</i> , <i>c</i> (Å)	12.2216 (8), 7.7932 (5), 20.6401 (14)	15.7007 (6), 10.2574 (6), 15.7422 (7)
α, β, γ (°)	97.948 (4)	116.484 (2)
<i>V</i> (Å ³)	1947.0 (2)	2269.20 (19)
<i>Z</i>	4	4
Radiation type	Mo <i>K</i> α	Mo <i>K</i> α
μ (mm ⁻¹)	0.10	0.10
Crystal size (mm)	0.42 × 0.36 × 0.28	0.43 × 0.30 × 0.28
Data collection		
Diffractometer	Bruker Kappa APEXII CCD	Bruker Kappa APEXII CCD
Absorption correction	Multi-scan (<i>SADABS</i> ; Bruker, 2005)	Multi-scan (<i>SADABS</i> ; Bruker, 2005)
<i>T</i> _{min} , <i>T</i> _{max}	0.961, 0.970	0.965, 0.978
No. of measured, independent and observed [<i>I</i> > 2σ(<i>I</i>)] reflections	15646, 4238, 2415	17605, 4913, 3118
<i>R</i> _{int}	0.045	0.037
(sin θ/λ) _{max} (Å ⁻¹)	0.639	0.639
Refinement		
<i>R</i> [<i>F</i> ² > 2σ(<i>F</i> ²)], <i>wR</i> (<i>F</i> ²), <i>S</i>	0.053, 0.138, 1.00	0.055, 0.171, 1.06
No. of reflections	4238	4913
No. of parameters	285	311
H-atom treatment	H atoms treated by a mixture of independent and constrained refinement	H-atom parameters constrained
Δ _{max} , Δ _{min} (e Å ⁻³)	0.18, -0.17	0.34, -0.42

of amide moieties [N(3)-C(15) 1.339(2) Å in **5a** and N(3)-C(15) 1.361(2) Å in **5b**].

Selected bond lengths (Å): [N(3)-C(15) 1.339(2)Å; N(2)-C(14) 1.451(2)Å; N(3)-C(15) 1.339(2)Å; N(3)-N(4) 1.381(2)Å; N(4)-C(16) 1.279(2)Å] in **5a** and [N(3)-C(15) 1.361(2)Å; N(3)-C(15) 1.361(2)Å; N(3)-N(4) 1.369(2)Å; N(4)-C(16) 1.287(2)Å; N(5)-C(17) 1.367(3)Å in **5b**]. Selected dihedral angles (°): [N(4)-N(3)-C(15)-O(1) -174.86(18), N(4)-N(3)-C(15)-C(14) 5.7(3), N(4)-C(16)-C(18)-C(23) -13.7(3)] in **5a** and [N(4)-N(3)-C(15)-O(1) 175.42(19), N(4)-N(3)-C(15)-C(14) -3.3(3), N(4)-C(16)-C(19)-C(18) -176.7(2) in **5b**].

In the solid state packing,^[59–65] the amide moiety in both benzoimidazole-based hydrazones **5a** and **5b** adopt cis-conformation, providing the possibility of appearance

of a centrosymmetric amide dimer $R_2^2(8)\{\cdots\text{H-N-C=O}\}_2$ synthon. However, this dimeric synthon appeared in only compound **5a** [(N(3)-H(3)⋯O(1) 2.088 Å], facilitated by centrosymmetric CH⋯O interactions [(C(17)-H(17C)⋯O(1) 2.353 Å] (Figure 2a). In comparison, the amide moieties of two centrosymmetric molecules of **5b** are bridged by methanol molecules [(N(5)-H(5A)⋯O(3) 1.945 Å, (C(25)-H(25B)⋯O(2) 2.436 Å] in the solid state packing of benzoimidazole-based hydrazones **5b** (Figure 2b). The CH⋯F [(C(20)-H(20)⋯F(1A) 2.589 Å], CH⋯N [(C(17)-H(17B)⋯N(1) 2.651 Å] and CH⋯π [(C(22)-H(22)⋯C(12) 2.90 Å] interactions in **5a** and the CH⋯F[(C(3)-H(3)⋯F(1) 2.618 Å], OH⋯N [(O(3)-H(3B)⋯N(1) 1.975 Å] and CH⋯π [(C(11)-H(11)⋯C(6) 2.888 Å] interactions in **5b** are the other notable non-

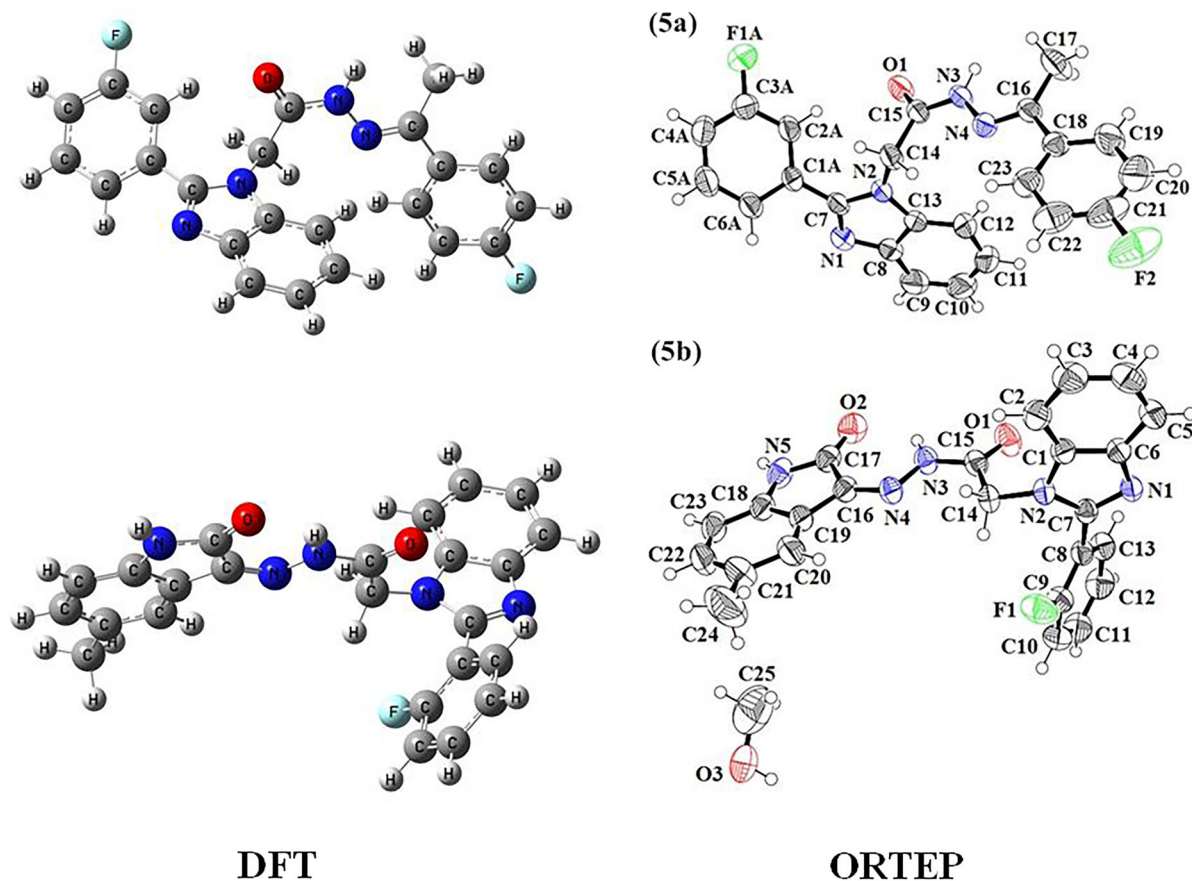


FIGURE 1 The molecular structures (DFT and ORTEP diagram) of benzoimidazole-based hydrazones a) **5a**; and b) **5b**

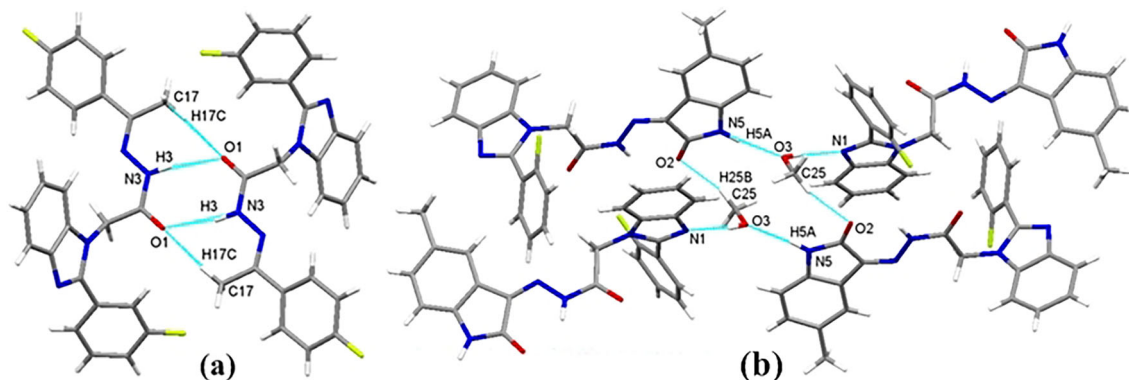


FIGURE 2 Showing a) centrosymmetric amide dimer $R_2(8)\{\dots H-N-C=O\}_2$ synthon in the solid state structure of **5a**; a) the centrosymmetric molecules of **5b** bridged by methanol molecules

covalent interactions in the 3D-packing of these compounds (Figure 3).

3.3 | Computational studies

3.3.1 | Geometric structures

In order to evaluate geometrical parameters including bond angles and bond lengths of **5a** and **5b**, SC-XRD

driven structures were used initially for the geometry optimization. The optimized molecular structures of **5a** and **5b** are depicted in Figure 1. Atom numbering scheme of **5a** and **5b** as shown in Figures S1-S2 (Supplementary information) was used to elucidate the geometrical parameters from SC-XRD and DFT structures and results are collected in Tables S1 and S2 (Supplementary information) respectively. A comparison between SC-XRD and DFT calculated bond lengths and bond angles have been made which indicates that SC-XRD findings

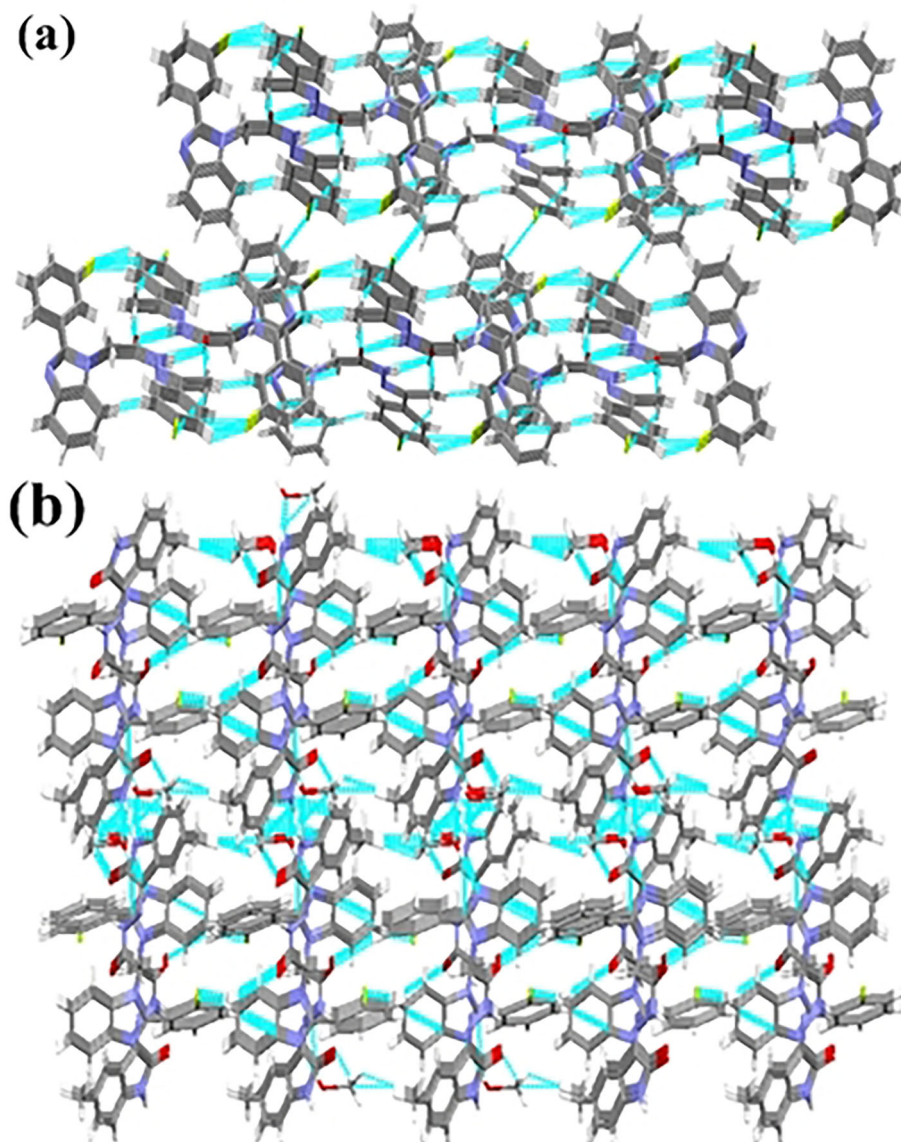


FIGURE 3 Showing, a) 3D-solid state packing in **5a**; b) 3D-solid state packing in **5b**

coincide nicely with corresponding DFT generated parameters. Overall, 0.038 ± 0.025 Å and 0.031 ± 0.022 Å are the ranges of deviation found in bond lengths of **5a** and **5b** respectively. Similarly, bond angles in **5a** and **5b** are deviated in the ambient of $2.4^\circ \pm 2.1^\circ$ and $1.6^\circ \pm 1.1^\circ$ respectively. In **5a**, bond lengths between fluorine (F) and carbon (C) atoms of F(1)-C(10) and F(2)-C(28) are measured as 1.360 Å, 1.363 Å through DFT and 1.342 Å, 1.338 Å through XRD respectively. On the other hand in **5b**, C-F bond length is found to be 1.354 Å (DFT) and 1.349 Å (XRD) for F(1)-C(17). The oxygen-carbon (O-C) bond length in **5a** is noted as 1.230 Å through DFT which are in good agreement with XRD calculated O-C bond length value 1.214 Å for O(3)-C(22). Similarly in **5b**, DFT computed O-C bond length values 1.216 Å, 1.220 Å for O(7)-C(23) and O(8)-C(25) are strongly supported by XRD calculated values 1.207 Å, 1.219 Å

respectively. The nitrogen (N)-carbon (C) bond length values for N(4)-C(14), N(4)-C(15), N(5)-C(20), N(5)-C(21), N(6)-N(7), N(6)-C(22), N(7)-C(23) in **5a** are calculated as 1.308 Å, 1.382 Å, 1.373 Å, 1.445 Å, 1.381 Å, 1.335 Å, 1.278 Å and 1.309 Å, 1.381 Å, 1.382 Å, 1.444 Å, 1.358 Å, 1.374 Å, 1.284 Å through DFT and XRD respectively. Similarly in **5b**, a good agreement is found between DFT and XRD measured values for bond lengths of N(2)-C(14), N(2)-C(15), N(3)-C(9), N(3)-C(15), N(3)-C(22), N(4)-N(5), N(4)-C(23), N(5)-C(24), N(6)-C(25), N(6)-C(26) found as 1.390 Å, 1.317 Å, 1.386 Å, 1.374 Å, 1.458 Å, 1.369 Å, 1.360 Å, 1.288 Å, 1.366 Å, 1.402 Å through DFT and 1.383 Å, 1.306 Å, 1.384 Å, 1.382 Å, 1.438 Å, 1.338 Å, 1.384 Å, 1.285 Å, 1.372 Å, 1.406 Å through XRD respectively. In **5a**, the calculated bond angles between F(1)-C(10)-C(9), (F1)-C(10)-C(11), F(2)-C(28)-C(27) and F(2)-C(28)-C(29) are found to be 118.5° ,

118.1°, 118.9°, 118.8° (DFT) and 118.6°, 118.7°, 119.1°, 118.9° (XRD) respectively. Similarly in **5b**, DFT and XRD calculated bond angles for F(1)-C(17)-C(16), F(1)-C(17)-C(18) are measured as 118.1°, 118.6° and 119.0°, 118.3° respectively. The calculated bond angles for different C-N atoms in **5a** are observed in the range of 105.2°-131.3° through DFT which are strongly supported by corresponding XRD results found in the span of 105.2°-131.7°. Similarly in **5b**, DFT calculated bond angles range 105.3°-132.3° for different C-N atoms are found in accordance with the XRD results range 104.9°-129.3° respectively (see Tables S1 and S2 (Supplementary Information)).

In a nutshell from preceding discussion, good concurrence between structural parameters estimated via XRD and DFT studies are observed.

3.4 | Natural bond orbitals (NBO) analysis

Natural bond orbital (NBO) approach is seen as one of the decent techniques which plays a critical commitment to examining inter and intra-molecular hydrogen

bonding.^[66] Additionally, it demonstrates amazing interpretation of conjugative interaction and charge transformation phenomenon of molecules. The second order stabilization energy, the filled and vacant orbitals can be explained by NBO approach.^[67,68] The second order stabilization energy $E^{(2)}$ has laid on the line association to the intensity of energy between donor and acceptor. The second order stabilization energy $E^{(2)}$ can be defined by Equation 1.

$$E^{(2)} = q_i \frac{(F_{i,j})^2}{\epsilon_j - \epsilon_i} \quad (1)$$

Where q_i is donor orbital occupancy, ϵ_j and ϵ_i are diagonal element and $F(i,j)$ is off-diagonal NBO fock matrix element. The second order perturbation theory analysis display diverse description of hyperconjugative interactions as can be seen in Tables S3 and S4 (Supplementary Information). Tables S3 and S4 show many sorts of non-covalent interactions (NCIs). The optimized geometry for dimmers of **5a** and **5b** applying M06-2X/6-31G(d,p) level of theory showing atom labels is represented in Figure 4. The hydrogen bonding (HB) is one of most attentive

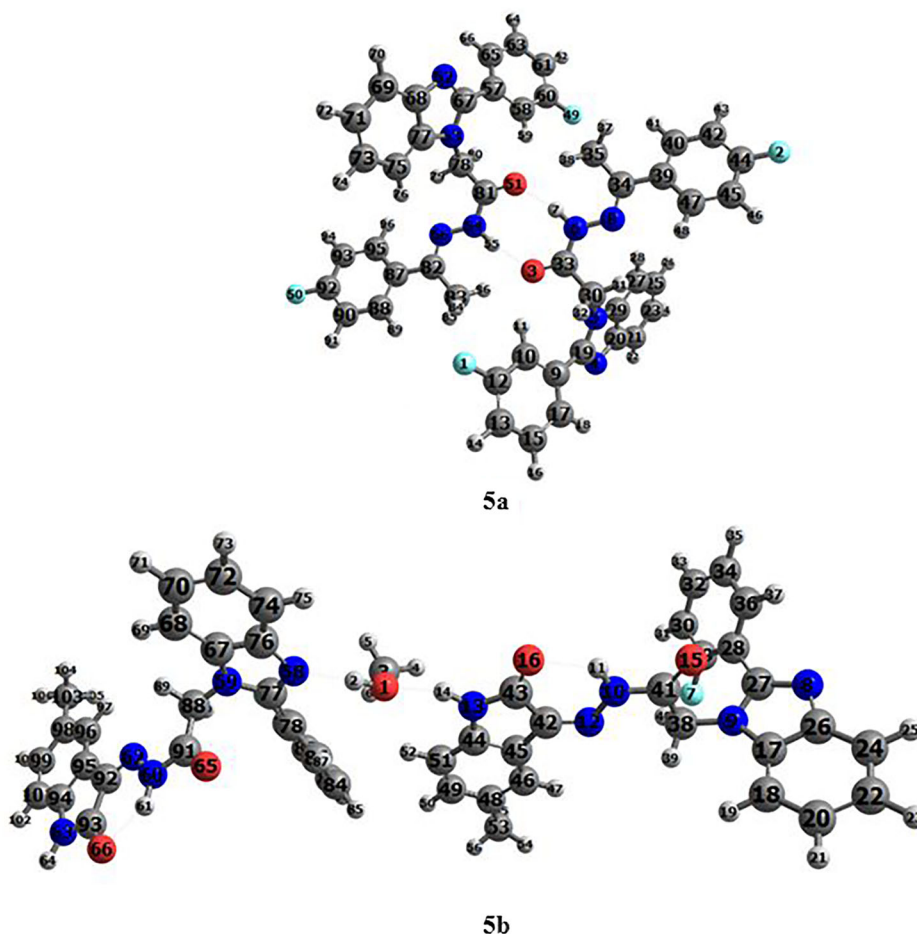


FIGURE 4 The optimized geometry of dimmers of **5a** and **5b** applying M06-2X/6-31G(d,p) method showing atom labels

interactions which is observed in the dimeric structure (**5a**), owing to the delocalization of the lone pair of O1LP(1) and O1'LP(1) to the antibonding sigma orbitals (σ^*) of N3'-H3' and N3-H3 respectively. Consequently, the stabilization energy as 10.38 kcal/mol is observed in both hydrogen bonds (Table S3). Dimeric structure (**5b**) likewise involves the hydrogen bond (HB). This HB is the result of delocalization of the lone pair of O3LP(2) and N1'LP(1) to the σ^* of N5-H5A and O3-H3B respectively. In these cases, the stabilization energies are reported to be 10.90 and 26.80 kcal/mol respectively (Table S4). Therefore, on the basis of bond evidence, it is concluded that both dimers of investigated compounds **5a** and **5b** have a synchronism between the XRD and NBO findings.

Apart from the inter-molecular H-bonds (H.B), other kinds of donor-acceptor intra-molecular charge transfer (ICT) interplay is also noticed in **5a** transitions i.e. $\pi(N1-C7) \rightarrow \pi^*(C8-C13)$, $\pi(C1-C2) \rightarrow \pi^*(C8-C13)$, $\pi^*(C3-C4)$ and $\pi^*(C5-C6)$, $\pi(C3-C4) \rightarrow \pi^*(C5-C6)$, $\pi(C5-C6) \rightarrow \pi^*(C1-C2)$ and $\pi^*(C3-C4)$ and $\pi(C18-C23) \rightarrow \pi^*(N1-C7)$ which contain 24.27, 14.04, 31.79, 24.83, 28.05, 30.47, 27.61 and 19.34 kcal/mol stabilization energy values respectively. These transitions endorse the effective delocalization of the electrons of imidazole to the benzenes ring. Moreover, F1LP(1) $\rightarrow \pi^*(C3-C4)$ and $\pi^*(C20-C21)$, N1LP(1) $\rightarrow \pi^*(N2-C7)$, N2LP(1) $\rightarrow \pi^*(N1-C7)$ and $\pi^*(C8-C13)$, N3LP(1) $\rightarrow \pi^*(O1-C15)$ and $\pi^*(N4-C16)$ consist of 22.23, 24.31, 13.33, 60.55, 41.82, 93.09 and 29.61 kcal/mol stabilization energy value which indicate a strong delocalization of the lone pairs of fluorides, carbonyl functional group and N=N double bond to the benzene rings in **5a** (Table S3).

With respect to the crystal **5b**, the following transitions $\pi(N4-C16) \rightarrow \pi^*(O2-C17)$, $\pi(C4-C5) \rightarrow \pi^*(C2-C3)$, $\pi(C8-C9) \rightarrow \pi^*(C10-C11)$ and $\pi^*(C12-C13)$, $\pi(C10-C11) \rightarrow \pi^*(C8-C9)$ and $\pi^*(C12-C13)$, $\pi(C12-C13) \rightarrow \pi^*(C8-C9)$ and $\pi^*(C10-C11)$, $\pi(C18-C23) \rightarrow \pi^*(C19-C20)$ and $\pi^*(C21-C22)$, $\pi(N'-C7') \rightarrow \pi^*(C1'-C6')$ and $\pi(N4'-C16') \rightarrow \pi^*(O2'-C17')$ and $\pi^*(C19'-C20')$ contain 13.67, 27.83, 26.35, 27.88, 32.15, 24.18, 26.63, 33.24, 25.24, 30.21, 22.89, 14.41 and 10.46 kcal/mol stabilization energy value respectively. Furthermore, resonance of lone pairs is also observed in **5b** confirmed through transition i.e. F1'LP(1) $\rightarrow \pi^*(C8'-C9')$, O1'LP(1) $\rightarrow \sigma^*(C14'-C15')$, O2'LP(1) $\rightarrow \sigma^*(N5'-C17')$ and $\sigma^*(C16'-C17')$, N3'LP(1) $\rightarrow \pi^*(N4'-C16')$ and $\pi^*(O1'-C15')$, N5'LP(1) $\rightarrow \pi^*(O2'-C17')$ and $\pi^*(C18'-C23')$ hold 22.52, 27.62, 32.13, 23.41, 47.14, 63.93, 79.38 and 41.59 kcal/mol energy value (Table S4) which also endorse the effective delocalization of the electrons of

imidazole, the lone pairs of fluorides, carbonyl functional group and nitrogen bond to the entire system.

It might be inferred that hydrogen bonding and the hyper conjugative interactions are pivotal cause for the existence of investigated compounds **5a** and **5b** in the solid-state.

3.5 | Mulliken atomic charges

determined at M06-2X methods with different basis set 6-31G(d,p) and 6-311G(2d,p) as can be seen in Figure 5. The calculated Mulliken atomic charges are summarized in Table S5 (Supplementary Information). The phenomenon associating the electronegativity equalization^[69,70] and charge transformation process takes place in reactions to obtain the electrostatic potential on external surfaces of systems and can be explained through Mulliken population examination.^[71] The electronic charges of atoms play a vital role in the molecular conformation and bonding capability.^[72] The data of Mulliken population reveals that the presence of more electronegative atoms such as F, O and N in both compounds (**5a** and **5b**) make unequal redistribution of the electron density over the benzene rings. The theoretically determined Mulliken atomic charge of oxygen atoms are found to be as 3O(-0.397991e) in **5a** and 9O(-0.214285e), 10O(-0.451386e) in **5b** respectively. On the other hand, the Mulliken charge of H7 and H8 are found to be 0.188501e and 0.296733e in **5a** and **5b** respectively as shown in Table S5 (Supplementary Information). Subsequently, Mulliken atomic charges confirm the attendance of hydrogen bonds for C=O3'7H-N and C=O9'8H-N in **5a** and **5b** respectively; which are in good agreement to the experimental and NBO findings (Figure 5). This data show that the magnitude of Mulliken atomic charges depend on the basis set as shown in Figure 5, however, the tendency of atomic charges is same in both basis sets.

3.6 | FT-IR analysis

The nature of vibrational modes present in **5a** and **5b** was explored by performing gas phase DFT calculations at M06-2X/6-31G(d,p) functional. The DFT computed FT-IR spectrum of **5a** and **5b** (monomer and dimers) along with their experimentally calculated spectrum is depicted in Figures S5-S6 and S7 (Supplementary Information) respectively. The investigated compounds **5a** and **5b** consist of -CH₃, -CH₂, C-C, C=C, C=O, C=N-NH, and F groups.

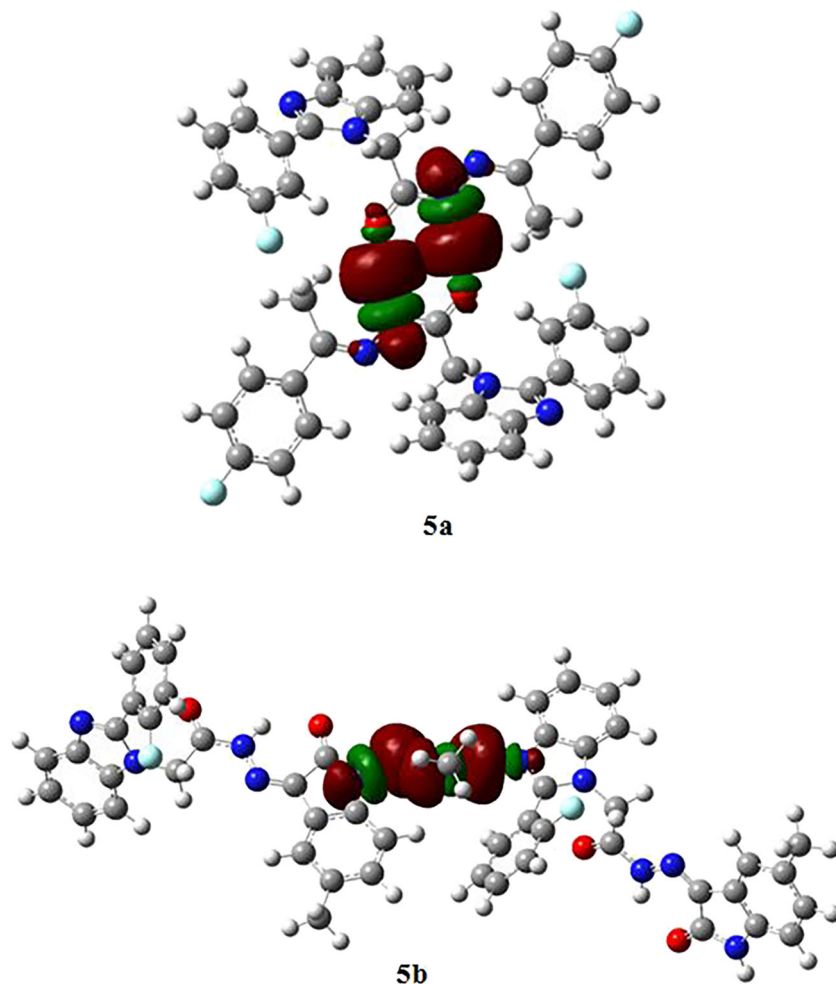


FIGURE 5 Hydrogen bond interactions in dimers **5a** and **5b** are constructed by donor–acceptor interaction between the lone pair orbitals and the anti-bonding orbitals

3.7 | C–H vibrations

The aromatic C–H stretching vibrations are calculated at 3246 cm^{-1} to 3201 cm^{-1} which occur in the characteristic region of the aromatic C–H stretching vibrations.^[73] The asymmetric and symmetric stretching modes of the methyl groups generally appear in the ambient of 3100 to 2880 cm^{-1} . In our study, bands observed at 3130 cm^{-1} and 3065 cm^{-1} were assigned to asymmetric and symmetric vibrational modes in **5a**. Similarly in **5b**, asymmetric and symmetric stretching vibrations are found with wave numbers at 3166 cm^{-1} and 3070 cm^{-1} , respectively.

CH_2 vibrational bands in **5a** were aroused due to the asymmetric and symmetric mode of vibrations observed at 3184 cm^{-1} and 3123 cm^{-1} , respectively. On the other hand in **5b**, wavenumbers observed at 3186 cm^{-1} and 3136 cm^{-1} were due to the asymmetric and symmetric stretching vibrations.

3.8 | C–C stretching vibration

Literature study uncovers that the peaks due to C=C stretching vibrations normally occurs with medium

intensity in the region of 1680 to 1620 cm^{-1} in the IR spectra.^[74] In our study, bands observed at 1682 to 1722 cm^{-1} in **5b** and 1675 to 1715 cm^{-1} in **5a** are assigned to these vibrations.

The C=O symmetric stretching band frequency appeared to be at 1848 cm^{-1} and $1856, 1881\text{ cm}^{-1}$ for monomer of **5a** and **5b** respectively. Whereas, stretching band frequency for dimers of compounds **5a** and **5b** were found at 1798 cm^{-1} and 1860 cm^{-1} respectively which are little bit larger than experimentally determined frequencies [1672 cm^{-1} (**5a**) and 1690 cm^{-1} (**5b**)]. This observed difference might because of the more polar carbonyl functional group which can be associated different types of molecular interaction in the solid phase.

3.9 | N–H group vibration

The N–H stretching vibration of the secondary amines appeared around 3500 – 3000 cm^{-1} in the IR absorption spectra.^[73] According to our findings, the N–H stretching modes are observed to be at 3565 cm^{-1} and 3692 cm^{-1} for monomers of **5a** and **5b**, respectively. On the other hand,

the N-H vibrations of their dimers have been observed at 3383 cm^{-1} and 3424 cm^{-1} with high intensity and presence of broad band showing good agreement to the experimental N-H values of **5a** and **5b** found at 3374 cm^{-1} and 3421 cm^{-1} respectively. This is because of the existence of intramolecular hydrogen bonding.^[75] The same finding has been proved in NBO study which is also in good agreement with experimental one as can be seen in Figure 6.

3.10 | C-N stretching vibration

The stretching vibrations for C-N group is found to be at 1615 cm^{-1} in **5a** which are strongly supported by experimental C-N group value observed at 1611 cm^{-1} . Similarly in **5b**, the DFT computed C-N vibrations with wave number at 1625 cm^{-1} is comparable with experimental measured C-N vibrations 1623 cm^{-1} .

From preceding discussion, it is well evident that the results obtained from experimental and computed FT-IR are in very good agreement and confirm the functional groups and hydrogen bonds.

3.11 | UV-visible study

In order to have photophysical insights about the probability of charge transfer, contributing configurations to the transitions and nature of electronic transitions within **5a** and **5b**, UV-Vis spectrum of **5a** and **5b** was recorded both experimentally (in solvent phase such as 1,4-dioxane, acetone, dimethyl sulfoxide (DMSO)) and computationally using time-dependent density functional theory (TD-DFT) at M06-2X/631G(d,p) level of theory. The experimental UV-Vis spectrum of **5a** and **5b** are displayed in Figure S8 (Supplementary Information). Similarly, TD spectrum of **5a** and **5b** obtained from TDDFT calculation are depicted in Figure S9 (Supple-

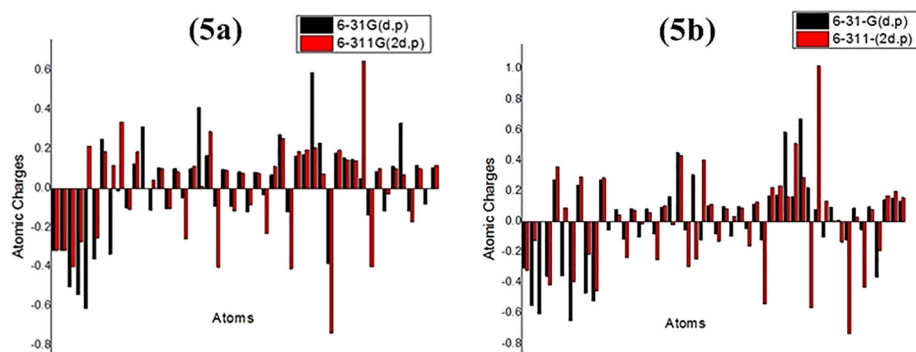


FIGURE 6 The Mulliken atomic charge distribution of compounds **5a** and **5b**

TABLE 2 Wave length, excitation energy and oscillator strength for **5a** and **5b**

Compounds	Expt. λ <i>max</i> (nm)	Cal. λ <i>max</i> (nm)	E^{DFT} (eV)	f	MO contributions
5a	281.80 ^a	249.81	4.9628	0.0035	H-3 \rightarrow L(17%), H-7 \rightarrow L + 5 (14%), H-1 \rightarrow L (28%), H-9 \rightarrow L(5%), H-9 \rightarrow L + 4(3%), H-9 \rightarrow L + 5(6%), H-7 \rightarrow L + 4(8%), H \rightarrow L(4%)
	293.40 ^b	244.43	5.0721	0.3864	H-1 \rightarrow L + 1(25%), H \rightarrow L + 1 (54%), H-1 \rightarrow L + 4 (2%), H-1 \rightarrow L + 6(5%), H \rightarrow L + 4(2%)
	283.60 ^c	240.24	5.1605	0.7011	H-2 \rightarrow L(89%), H-1 \rightarrow L + 1 (3%),
5b	337.00 ^a	331.69	3.7377	0.1314	H-2 \rightarrow L(94%), H-4 \rightarrow L(2%)
	330.40 ^b	315.64	3.9277	0.0007	H-8 \rightarrow L(57%), H-7 \rightarrow L(18%), H-9 \rightarrow L (3%), H-8 \rightarrow L + 2(2%), H-1 \rightarrow L(8%),
	333.80 ^c	298.25	4.1568	0.0015	H \rightarrow L(98%),

E = Excitation energy (eV); λ =wave length (nm); f = oscillator strength; MO = molecular orbitals; H = HOMO, L = LUMO; λ (nm); Expt. = Experimental; Cal. = DFT Calculated; a = 1,4-dioxan, b = acetone, c = DMSO

mentary Information). However, the vertical excitation energies, absorption peak (λ_{max}), oscillator strength (f) are reported in Table 2.

The experimental UV–visible spectra of **5a** and **5b** are dominated by π - π transitions. These transitions occur in the short wavelength UV region at 281.80 nm, 293.40 nm and 283.60 nm for compound (**5a**) in 1,4-dioxan, acetone and DMSO respectively. Whereas, the transitions occur in the longer wavelength UV region in the case of compound (**5b**) such as 337.00 nm, 330.40 nm and 333.80 nm in 1,4-dioxan, acetone and DMSO, respectively, which show excellent agreement to the DFT determined wave length [λ_{max} 331.69]. The longer wavelength UV region of **5b** because of the stronger bathochromic shift (red shift) which is the evidence of less number of fluoride substitutes in the case of **5b** as compared to **5a**. The reasonable agreement between DFT and experimental data confirms the purity of both compounds. Additionally, we observed forbidden transitions in both compounds using TD-DFT where, the magnitude of the oscillator strength is very weak which is usually difficult to observe in experimental analysis (Table 2).

3.12 | Frontier molecular orbital analysis

The energies of the highest occupied molecular orbital (HOMO) and lowest unoccupied molecular orbital (LUMO) are calculated through M06-2X with basis set [6-31G(d,p)] and results are summarized in Table 3. The influence of deactivating F group groups on FMOs of **5a** and **5b** is described in pictorial display of FMOs shown in Figure 7. The energy gap value 4.971 eV of **5b** is found to be smaller than **5a** value 6.504 eV. The smaller energy gap in **5b** is due to the presence of one F group on the architecture. On the other hand in **5a**, two F groups are attached on opposite positions and different benzene rings of the structure which mutually influence the charge withdrawing capability of these groups, hence, leading to larger energy gap value.

The chemical potential (μ), global hardness (η), global softness (S), global electrophilicity index (ω), electron affinity (EA), electronegativity (X) and ionization potential (IP) have been contemplated as global reactivity parameters^[76–79] and are proven as very effective descriptors for biological activity and optoelectronic applications. The global reactivity descriptors were obtained using the

TABLE 3 Computed energies (E) for **5a** and **5b**

5a		5b		
MO(s)	E (eV)	E (eV)	E (eV)	E (eV)
HOMO	-7.184	6.504	-6.817	4.971
LUMO	-0.664		-1.846	

E = energy, E (eV) = $E_{LUMO} - E_{HOMO}$; MO, molecular orbital

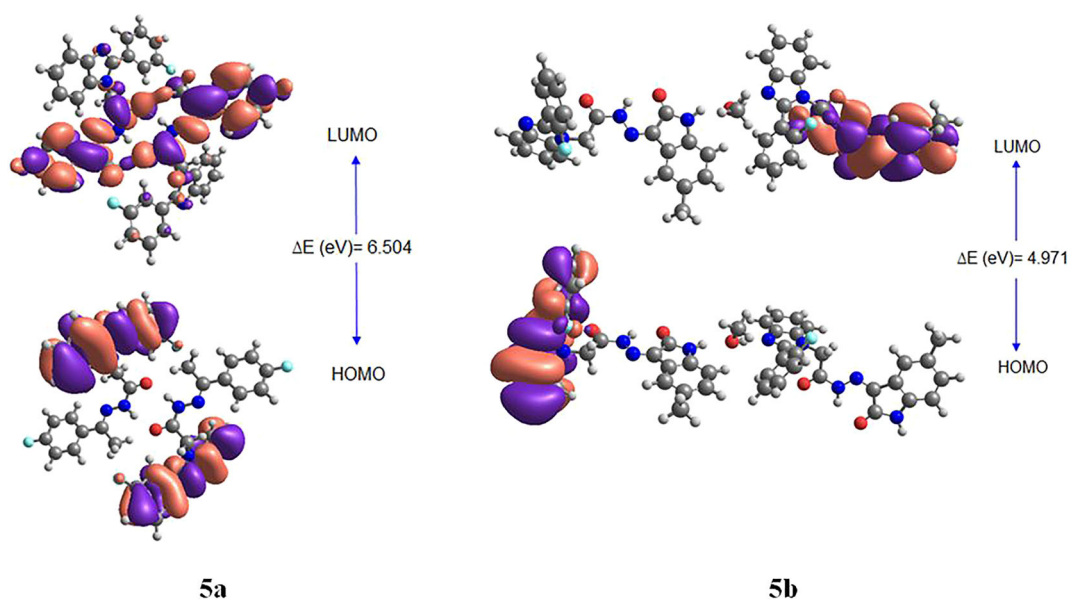


FIGURE 7 Frontier molecular orbitals for dimer of compound **5a** and **5b**

TABLE 4 Ionization potential (I), electron affinity (A), electronegativity (X), global hardness (η), chemical potential (μ), global electrophilicity (ω) and global softness (s)

	I	A	X	H	μ	ω	s
5a	7.184	0.664	3.924	3.260	-3.924	2.361	0.153
5b	6.817	1.846	4.331	2.485	-4.331	3.774	0.201

energies of LUMO, HOMO and by taking the advantage of equations mentioned in the supplementary information, and results are tabulated in Table 4.

The reactivity and the selectivity parameters of investigated compounds can be assessed working with the global reactivity descriptors. The electron affinity, ionization potential and electronegativity are well-known parameters in physical organic chemistry.^[80] The small & high energy difference between HOMO & LUMO reveals a malleableness and firmness of investigated species respectively. The negative chemical potential discloses the stability of the systems. Table 4 uncovers that the magnitude of hardness is greater than softness in both compounds, which means that both molecules have high stability. The negative magnitude of chemical potential also provides strengthen to the stability and inclination towards decomposition into its elements cannot be possible easily with the exception of external force. Positive value of six MOs of **5a** and **5b** represents that both investigated compounds can contribute in charge transfer reaction. The electron donating strength of **5a** is found to be greater than **5b** as indicated by greater *I* value respectively. On the other hand, *A* value of **5b** is observed greater in magnitude than **5a** indicating its greater accepting aptitude. Overall, *I*, *X* and ω value of

5b is found greater than **5a**. The information obtained from the global reactivity descriptors suggests that both compounds are stable and might participate in charge transfer reactions. Particularly **5b** due to its smaller energy gap, greater softness and electron affinity than **5a** can play a vital role for biological and optoelectronic applications.

3.13 | Nonlinear optical (NLO) properties

To predict the NLO properties of synthesized compounds **5a** and **5b**, DFT calculations were performed at M06-2X/631G(d,p) level of theory. The diagonal elements of equation 2 are utilized for estimating the average polarizability (α) values.

$$\langle \alpha \rangle = 1/3(\alpha_{xx} + \alpha_{yy} + \alpha_{zz}) \quad (2)$$

First (β_{tot}) and second hyperpolarizability γ values are measured utilizing equations 3 and 4 respectively.

$$\beta_{tot} = [(\beta_{xxx} + \beta_{xyy} + \beta_{xzz})^2 + (\beta_{yyy} + \beta_{xxy} + \beta_{yzz})^2 + (\beta_{zzz} + \beta_{xxz} + \beta_{yyz})^2]^{1/2} \quad (3)$$

$$\gamma = \frac{1}{5}(\gamma_{xxxx} + \gamma_{yyyy} + \gamma_{zzzz} + 2[\gamma_{xxyy} + \gamma_{yyzz} + \gamma_{xxzz}]) \quad (4)$$

The results for the dipole moment, linear polarizability, first hyperpolarizability and second hyperpolarizability of **5a** and **5b** are tabulated in Table 5. The total first hyperpolarizability and second hyperpolarizability values are presented in electrostatic unit (esu).^[81-83] Dipole

TABLE 5 The dipole moment (D) and computed dipole polarizabilities (esu), first and second hyperpolarizabilities (esu) for **5a** and **5b**

	5a	5b		5a	5b		5a	5b
μ_x	5.3286	-8.3275	β_{xxx}	35.024	-318.280	γ_{xxxx}	-14482.930	-13911.400
μ_y	-2.8906	0.6046	β_{xyy}	-47.123	-106.797	γ_{yyyy}	-3821.209	-4153.089
μ_z	0.4548	1.4940	β_{xzz}	-125.830	-71.318	γ_{zzzz}	-1458.479	-2318.741
M	6.0792	8.4820	β_{yyy}	282.896	-11.943	γ_{xxyy}	-3277.439	-3294.566
α_{xx}	391.4809	385.2935	β_{xxy}	-22.936	-157.500	γ_{zzxx}	-2670.715	-2789.813
α_{yy}	257.4865	293.2138	β_{yzz}	19.645	-35.791	γ_{yyzz}	-900.485	-1159.885
α_{zz}	183.7122	220.3757	β_{zzz}	134.894	-8.374	$\gamma \times 10^{-28}$ (esu)	-1.94	-2.01
$\alpha_{total} \times 10^{-23}$ (esu)	4.11	4.44	β_{xxz}	14.955	32.641			
			β_{yyz}	37.252	27.227			
			β_{xyz}	17.664	13.124			
			$\beta_{tot} \times 10^{-30}$ (esu)	3.14	4.66			

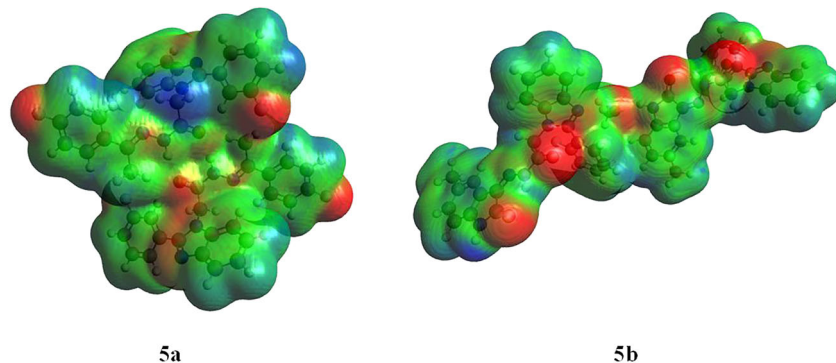


FIGURE 8 The molecular electrostatic potential (MEP) diagrams for dimers of **5a** and **5b**

moment is an important parameter that describes the interaction among atoms. It is the product of magnitude of charges and distance between them. The values for distribution of charges in x, y, and z-directions are listed in Table 5. The results point out that dipole moment value is noticed greater as 8.4820 D in **5b** than **5a** value 6.0792 D. Total dipole moment of urea molecule is 1.3732 D^[84] which is considered as standard molecule for comparing dipole moment and β_{tot} results. The dipole moments of **5a** and **5b** are calculated 4.42 and 6.17 times greater than urea molecule.

The results of major polarizability tensors of x, y, and z-directions and total linear polarizability are tabulated in Table 5. The results reveal that the dipole polarizability tensors value of **5b** is found higher in y and z-axis direction and slightly smaller in x-axis direction than polarizability tensors values **5a**. Overall, computed dipole polarizability value 4.44×10^{-23} (esu) is found to be higher in **5b** as compared to the lower value of dipole polarizability (4.41×10^{-23} (esu)) observed in **5a**.

The values of total first hyperpolarizability (second order polarizability or second order NLO; β_{tot}) and its contributing tensors are mentioned in Table 5. Higher and lower β_{tot} values are computed to be 3.14×10^{-30} (esu) and 4.66×10^{-30} (esu) in **5a** and **5b** respectively. The answer to the greater NLO activity of **5b** over **5a** is hidden in the basic structures of **5b**.

The smaller energy gap in **5b** is due to the presence of one F group on the architecture. On the other hand in **5a**, two F groups are attached on opposite positions and different benzene rings of the structure which mutually influence the charge withdrawing capability of these groups, hence, leading to larger energy gap value. The backbone of **5b** structure contains one F group. While in **5a**, two F groups are attached on opposite positions and different benzene rings which mutually influence the charge withdrawing capability of these groups. Therefore, delocalization of electrons and charge transfer increases in **5b**, which results in smaller energy gaps and greater NLO response of **5b** as compared to **5a**. Since urea molecule is used as reference material for

comparative NLO analysis.^[84] Therefore, β_{tot} values of **5a** and **5b** have been compared with urea molecule (β_{tot} (urea) = 0.372×10^{-30} esu). The β_{tot} values of **5a** and **5b** are computed 8.44 and 12.52 times greater than the urea molecule respectively. The values of second hyperpolarizability $\langle \gamma \rangle$ along with their contributing tensors are presented in Table 5. The $\langle \gamma \rangle$ of **5a** and **5b** is found to be -1.94×10^{-28} (esu) and -2.01×10^{-28} (esu) respectively. Overall, urea molecule comparative analysis evident that **5a** and **5b** are brilliant candidates for NLO properties associated hi-tech applications.

Molecular Electrostatic potential (MEP) analysis.

The three dimensional (3D) plot of entire electron density of investigated system is known as a molecular electrostatic potential (MEP) which can be evaluated by equation 5.

$$V(r) = \sum \left(\frac{Z_A}{R_A} - r \right) - \int (\rho(r')/r' - r) dr' \quad (5)$$

Where; the $V(r)$ is molecular electrostatic potential, Z_A stands for the magnitude of charge density over nucleus, A placed at R_A , $\rho(r')$ defines the electronic density function and r' is the integration variable.^[85,86] The applicability of MEP is to understand the reactivity such as electrophilic and nucleophilic attack as well as to explain the non-covalent interactions.^[87,88] The representation of MEP also explains positive, negative and neutral electrostatic potential with the help of color grading and the molecular size as well as shape.^[89] The red color is showing a possibility of the electrophilic attack and blue color is indicating the possibility of nucleophilic attack on the surface of investigated systems **5a** and **5b** as shown in Figure 8. The magnitude of electrostatic potential is enhancing by following order; red < orange < yellow < green < blue.^[90] As can be seen in the Figure 8, the negative potential regions are displayed because of the oxygen atoms and the positive potential regions are displayed due to the hydrogen atoms, carbon atoms and ring systems. The reign of the green displays the neutral potential. Clear identification of red and blue colors in

MEP diagrams is found showing hydrogen bonding interactions which are in agreement with our experimental results as well as NBO analysis.

4 | CONCLUSIONS

Two novel benzoimidazole-based hydrazones with chemical formula $C_{23}H_{18}F_2N_4O$ (**5a**) and $C_{25}H_{22}FN_5O_3$ (**5b**) were successfully synthesized for the first time in excellent yield (81–85%) and characterized using spectroscopic techniques like infrared FT-IR, UV-Visible, 1H -NMR, ^{13}C -NMR, EIMS, elemental analysis and SC-XRD. The **5a** and **5b** were found with monoclinic crystal lattice and space groups $P2_1/n$ and $P2_1/c$ respectively. SC-XRD generated structural parameters (bond lengths, bond angles), spectroscopic UV-Vis and FT-IR results are observed in line and strongly supported by corresponding DFT findings. The FT-IR analysis confirmed the presence of functional groups and hydrogen bonding in **5a** and **5b**. The UV-Vis analysis indicated the red shift of absorption band in **5b** as compared to **5a** and revealed the occurrence of maximum excitations from $\pi \rightarrow \pi^*$ transitions. NBO analysis uncovered the effective delocalization of the electrons of imidazole, lone pairs of fluorides, carbonyl functional group and nitrogen bond to the entire systems of **5a** and **5b**. Furthermore, presence of hydrogen bonding and hyper conjugative interactions were confirmed through NBO analysis which is pivotal cause for the existence of **5a** and **5b** in the solid-state. Clear identification of red and blue colors in MEP diagrams is found showing hydrogen bonding interactions which are in agreement with our experimental results as well as NBO analysis. The global reactivity descriptors suggest that both compounds are stable and might participate in charge transfer reactions. Particularly **5b** due to its smaller energy gap, greater softness and electron affinity than **5a** can play a vital role for biological and optoelectronic applications. The urea molecule comparative analysis evident that **5a** and **5b** are brilliant candidates for NLO properties associated hi-tech applications.

ACKNOWLEDGEMENTS

The authors extend their appreciation to Deanship of Scientific Research at King Khalid University, Saudi Arabia for funding this work through Research Groups Project under grant number (R.G.P.1/93/40). Atualpa A. C. Braga, (grants # 2011/07895-8, 2015/01491-3 and 2014/25770-6) is thankful to Fundação de Amparo à Pesquisa do Estado de São Paulo for financial support. AACB (grant 309715/2017-2) also thanks the Brazilian National Research Council (CNPq) for financial support

and fellowships. This study was financed in part by the Coordenação de Aperfeiçoamento de Pessoal de Nível Superior - Brasil (CAPES) - Finance Code 001.

CONFLICT OF INTEREST

No conflicts declared.

ORCID

Muhammad Khalid  <https://orcid.org/0000-0002-1899-5689>

REFERENCES

- [1] L. Dinparast, H. Valizadeh, M. B. Bahadori, S. Soltani, B. Asghari, M.-R. Rashidi, *J. Mol. Struct.* **2016**, *1114*, 84.
- [2] E. Menteşe, S. Ülker, B. Kahveci, *Chem. Heterocycl. Compd.* **2015**, *50*, 1671.
- [3] L. Barasa, S. Yoganathan, *RSC Adv.* **2018**, *8*, 35824.
- [4] P. Jeyakkumar, L. Zhang, S. R. Avula, C.-H. Zhou, *Eur. J. Med. Chem.* **2016**, *122*, 205.
- [5] H.-Z. Zhang, G. L. Damu, G.-X. Cai, C.-H. Zhou, *Eur. J. Med. Chem.* **2013**, *64*, 329.
- [6] T.-T. Miao, X.-B. Tao, D.-D. Li, H. Chen, X.-Y. Jin, Y. Geng, S.-F. Wang, W. Gu, *RSC Adv.* **2018**, *8*, 17511.
- [7] T. Gungor, A. Fouquet, J. M. Teulon, D. Provost, M. Cazes, A. Cloarec, *J. Med. Chem.* **1992**, *35*, 4455.
- [8] T. Pan, X. He, B. Chen, H. Chen, G. Geng, H. Luo, H. Zhang, C. Bai, *Eur. J. Med. Chem.* **2015**, *95*, 500.
- [9] J. Akhtar, A. A. Khan, Z. Ali, R. Haider, M. S. Yar, *Eur. J. Med. Chem.* **2017**, *125*, 143.
- [10] A. T. Mavrova, K. K. Anichina, D. I. Vuchev, J. A. Tsenov, P. S. Denkova, M. S. Kondeva, M. K. Micheva, *Eur. J. Med. Chem.* **2006**, *41*, 1412.
- [11] N. K. Nandwana, R. P. Singh, O. P. Patel, S. Dhiman, H. K. Saini, P. N. Jha, A. Kumar, *ACS Omega* **2018**, *3*, 16338.
- [12] P. Sharma, D. Thummuri, T. S. Reddy, K. R. Senwar, V. Naidu, G. Srinivasulu, S. K. Bharghava, N. Shankaraiah, *Eur. J. Med. Chem.* **2016**, *122*, 584.
- [13] K. B. Puttaraju, K. Shivashankar, M. Mahendra, V. P. Rasal, P. N. V. Vivek, K. Rai, M. B. Chanu, *Eur. J. Med. Chem.* **2013**, *69*, 316.
- [14] A. G. Banerjee, N. Das, S. A. Shengule, R. S. Srivastava, S. K. Shrivastava, *Eur. J. Med. Chem.* **2015**, *101*, 81.
- [15] G. E. Miana, S. R. Ribone, D. M. Vera, M. Sánchez-Moreno, M. R. Mazziere, M. A. Quevedo, *Eur. J. Med. Chem.* **2019**, *165*, 1.
- [16] H. B. El-Nassan, *Eur. J. Med. Chem.* **2012**, *53*, 22.
- [17] E. Menteşe, F. Yılmaz, M. Emirik, S. Ülker, B. Kahveci, *Bioorg. Chem.* **2018**, *76*, 478.
- [18] Y. Ding, J. Chai, P. A. Centrella, C. Gondo, J. L. DeLorey, M. A. Clark, *ACS Comb. Sci.* **2018**, *20*, 251.
- [19] E. Menteşe, M. Emirik, B. B. Sökmen, *Bioorg. Chem.* **2019**, *86*, 151.

- [20] T. Kim, H. Y. Yang, B. G. Park, S. Y. Jung, J.-H. Park, K. D. Park, S.-J. Min, J. Tae, H. Yang, S. Cho, *Eur. J. Med. Chem.* **2017**, *125*, 1172.
- [21] X.-F. Wang, C.-C. Du, S.-B. Zhou, D.-Z. Wang, *J. Mol. Struct.* **2017**, *1128*, 103.
- [22] Y. Gong, H.-F. Shi, P.-G. Jiang, W. Hua, J.-H. Lin, *Cryst. Growth des.* **2013**, *14*, 649.
- [23] L. Zhang, X. M. Peng, G. L. Damu, R. X. Geng, C. H. Zhou, *Med. Res. Rev.* **2014**, *34*, 340.
- [24] A. Garai, S. Sasmal, K. Biradha, *Cryst. Growth des.* **2016**, *16*, 4457.
- [25] A. Garcia, H. Zou, K. R. Hossain, Q. H. Xu, A. Buda, R. J. Clarke, *ACS Omega* **2019**, *4*, 518.
- [26] T. Jella, M. Srikanth, R. Bolligarla, Y. Soujanya, S. P. Singh, L. Giribabu, *Dalton Transactions* **2015**, *44*, 14697.
- [27] S. Samadhiya, A. Halve, *Orient. J. Chem.* **2001**, *17*, 119.
- [28] M. Taha, N. H. Ismail, W. Jamil, H. Rashwan, S. M. Kashif, A. A. Sain, M. I. Adenan, M. Ali, F. Rahim, K. M. Khan, *Eur. J. Med. Chem.* **2014**, *84*, 731.
- [29] S. S. Bharadwaj, B. Poojary, S. K. M. Nandish, J. Kengaiah, M. P. Kirana, M. K. Shankar, A. J. Das, A. Kulal, D. Sannaningaiah, *ACS Omega* **2018**, *3*, 12562.
- [30] M. U. Khan, M. Khalid, M. Ibrahim, A. A. C. Braga, M. Safdar, A. A. Al-Saadi, M. R. S. A. Janjua, *J. Phys. Chem. C* **2018**, *122*, 4009.
- [31] M. R. S. A. Janjua, M. U. Khan, B. Bashir, M. A. Iqbal, Y. Song, S. A. R. Naqvi, Z. A. Khan, *Comp. Theor. Chem.* **2012**, *994*, 34.
- [32] M. R. S. A. Janjua, M. Amin, M. Ali, B. Bashir, M. U. Khan, M. A. Iqbal, W. Guan, L. Yan, Z. M. Su, *Eur. J. Inorg. Chem.* **2012**, *2012*, 705.
- [33] M. U. Khan, M. Ibrahim, M. Khalid, M. S. Qureshi, T. Gulzar, K. M. Zia, A. A. Al-Saadi, M. R. S. A. Janjua, *Chem. Phys. Lett.* **2019**, *715*, 222.
- [34] M. U. Khan, M. Ibrahim, M. Khalid, A. A. C. Braga, S. Ahmed, A. Sultan, *J. Cluster Sci.* **2019**, *1*.
- [35] M. U. Khan, M. Ibrahim, M. Khalid, S. Jamil, A. A. Al-Saadi, M. R. S. A. Janjua, *Chem. Phys. Lett.* **2019**, *719*, 59.
- [36] M. Shahid, M. Salim, M. Khalid, M. N. Tahir, M. U. Khan, A. A. C. Braga, *J. Mol. Struct.* **2018**, *1161*, 66.
- [37] M. Khalid, M. Ali, M. Aslam, S. H. Sumrra, M. U. Khan, N. Raza, N. Kumar, M. Imran, *Int. J. Pharm. Sci. Res.* **2017**, *8*, 457.
- [38] M. Ibrahim, M. Abbas, M. Khalid, M. N. Tahir, M. U. Khan, A. Hussain, A. Ullah, A. Hussain, *J. Chem. Soc. Pak.* **2018**, *40*, 749.
- [39] R. Jawaria, M. Hussain, M. Khalid, M. U. Khan, M. N. Tahir, M. M. Naseer, A. A. C. Braga, Z. Shafiq, *Inorg. Chim. Acta* **2018**.
- [40] M. Akram, M. Adeel, M. Khalid, M. N. Tahir, M. U. Khan, M. A. Asghar, M. A. Ullah, M. Iqbal, *J. Mol. Struct.* **2018**, *1160*, 129.
- [41] M. S. Ahmad, M. Khalid, M. A. Shaheen, M. N. Tahir, M. U. Khan, A. A. C. Braga, H. A. Shad, *J. Phys. Chem. Solids* **2018**, *115*, 265.
- [42] M. Khalid, M. Adeel, M. A. Ullah, M. U. Khan, M. N. Tahir, A. A. C. Braga, *J. Saudi Chem. Soc.* **2018**, *23*, 546.
- [43] M. N. Tahir, S. H. Mirza, M. Khalid, A. Ali, M. U. Khan, A. A. C. Braga, *J. Mol. Struct.* **2019**, *1180*, 119.
- [44] M. Haroon, M. Khalid, T. Akhtar, M. N. Tahir, M. U. Khan, M. Saleem, R. Jawaria, *J. Mol. Struct.* **2019**, *1187*, 164.
- [45] A. Jagadesan, G. Peramaiyan, T. Srinivasan, R. M. Kumar, S. Arjunan, *J. Cryst. Growth* **2016**, *436*, 40.
- [46] N. Vijayan, K. Nagarajan, A. M. Slawin, C. Shashidharan Nair, G. Bhagavannarayana, *Cryst. Growth des.* **2007**, *7*, 445.
- [47] S. Horiuchi, S. Ishibashi, S. Inada, S. Aoyagi, *Cryst. Growth des.* **2018**, *19*, 328.
- [48] A. S. Alp, G. Kilcigil, E. D. Özdamar, T. Çoban, B. Eke, *Turk. J. Chem.* **2015**, *39*, 42.
- [49] A. A. Braga, G. Ujaque, F. Maseras, *Organometallics* **2006**, *25*, 3647.
- [50] M. García-Melchor, A. A. Braga, A. Lledós, G. Ujaque, F. Maseras, *Acc. Chem. Res.* **2013**, *46*, 2626.
- [51] A. A. Braga, N. H. Morgon, G. Ujaque, F. Maseras, *J. Am. Chem. Soc.* **2005**, *127*, 9298.
- [52] M. J. Frisch, G. W. Trucks, H. B. Schlegel, G. Scuseria, M. A. Robb, J. R. Cheeseman, G. Scalmani, V. Barone, B. Mennucci, G. Petersson, H. Nakatsuji, M. Caricato, X. Li, H. P. Hratchian, A. F. Izmaylov, J. Bloino, G. Zheng, J. L. Sonnenberg, M. Hada, M. Ehara, K. Toyota, R. Fukuda, J. Hasegawa, M. Ishida, T. Nakajima, Y. Honda, O. Kitao, H. Nakai, T. Vreven, J. A. Montgomery, J. E. Peralta, F. Ogliaro, M. Bearpark, J. J. Heyd, B. E. K. N. Kudin, V. N. Staroverov, R. Kobayashi, J. Normand, K. Raghavachari, A. Rendell, J. C. Burant, S. S. Iyengar, J. Tomasi, M. Cossi, N. Rega, J. M. Millam, M. Klene, J. E. Knox, J. B. Cross, V. Bakken, C. Adamo, J. Jaramillo, R. Gomperts, R. E. Stratmann, O. Yazyev, A. J. Austin, R. Cammi, C. Pomelli, J. W. Ochterski, R. L. Martin, K. Morokuma, V. J. Zakrzewski, G. A. Voth, P. Salvador, J. J. Dannenberg, S. Dapprich, A. D. Daniels, O. Farkas, J. B. Foresman, J. V. Ortiz, J. Cioslowski, D. J. Fox, *Gaussian 09, Revision B.01.*, Gaussian, Inc., Wallingford, CT **2009**.
- [53] M. Walker, A. J. Harvey, A. Sen, C. E. Dessent, *J. Phys. Chem. A* **2013**, *117*, 12590.
- [54] V. A. Rassolov, M. A. Ratner, J. A. Pople, P. C. Redfern, L. A. Curtiss, *J. Comput. Chem.* **2001**, *22*, 976.
- [55] F. Weinhold, E.D. Glendening, NBO 5.0 program manual: natural bond orbital analysis programs, Theoretical Chemistry Institute and Department of Chemistry, University of Wisconsin, Madison, WI 53706 (**2001**).
- [56] R. Dennington, T. Keith, J. Millam, *GaussView, version 5*, Semichem Inc., Shawnee Mission, KS **2009**.
- [57] Avogadro, http://avogadro.cc/wiki/Main_Page.
- [58] ChemCraft, <http://www.chemcraftprog.com>.
- [59] A. Hameed, Z. Shafiq, M. Yaqub, M. Hussain, M. A. Hussain, M. Afzal, M. N. Tahir, M. M. Naseer, *New J. Chem.* **2015**, *39*, 9351.
- [60] A. Hameed, Z. Shafiq, M. Yaqub, M. Hussain, H. Ahmad, M. Tahir, M. Naseer, *New J. Chem.* **2015**, *39*, 6052.
- [61] R. Jawaria, M. Hussain, Z. Shafiq, H. B. Ahmad, M. N. Tahir, H. A. Shad, M. M. Naseer, *CrystEngComm* **2015**, *17*, 2553.
- [62] M. Hussain, R. Jawaria, Z. Shafiq, G. Abbas, M. M. Naseer, *J. Organomet. Chem.* **2017**, *846*, 121.

- [63] S. Malik, A. Khan, M. M. Naseer, S. U. Khan, A. Ashraf, M. Ashraf, M. Rafiq, K. Mahmood, M. N. Tahir, Z. Shafiq, *Bioorg. Chem.* **2019**, *84*, 372.
- [64] M. M. Naseer, M. Hussain, A. Bauzá, K. M. Lo, A. Frontera, *ChemPlusChem* **2018**, *83*, 881.
- [65] M. M. Naseer, A. Bauzá, H. Alnasr, K. Jurkschat, A. Frontera, *CrystEngComm* **2018**, *20*, 3251.
- [66] Ö. Tamer, D. Avci, Y. Atalay, *Spectrochim. Acta. A Mol. Biomol. Spectrosc.* **2014**, *117*, 78.
- [67] M. Szafran, A. Komasa, E. Bartoszak-Adamska, *J. Mol. Struct.* **2007**, *827*, 101.
- [68] C. James, A. A. Raj, R. Reghunathan, V. Jayakumar, I. H. Joe, *J. Raman Spectrosc.* **2006**, *37*, 1381.
- [69] R. Mulliken, R. S. Mulliken, *J. Chem. Phys.* **1955**, *23*, 1833.
- [70] R. G. Parr, R. G. Pearson, *J. Am. Chem. Soc.* **1983**, *105*, 7512.
- [71] L. Pauling, *The Nature of the Chemical Bond*, Cornell university press Ithaca, NY **1960** 482.
- [72] L. Li, C. Wu, Z. Wang, L. Zhao, Z. Li, C. Sun, T. Sun, *Spectrochim. Acta. A Mol. Biomol. Spectrosc.* **2015**, *136*, 338.
- [73] G. Varsányi, *Assignments for vibrational spectra of seven hundred benzene derivatives*, Halsted Press, New York **1974**.
- [74] G. Socrates, *Infrared and Raman characteristic group frequencies: tables and charts*, John Wiley & Sons, Chichester **2004**.
- [75] R. M. Silverstein, G. C. Bassler, *J. Chem. Educ.* **1962**, *39*, 546.
- [76] R. G. Parr, L. v. Szentpály, S. Liu, *J. Am. Chem. Soc.* **1999**, *121*, 1922.
- [77] R. G. Parr, R. A. Donnelly, M. Levy, W. E. Palke, *J. Chem. Phys.* **1978**, *68*, 3801.
- [78] P. K. Chattaraj, U. Sarkar, D. R. Roy, *Chem. Rev.* **2006**, *106*, 2065.
- [79] A. Lesar, I. Milošev, *Chem. Phys. Lett.* **2009**, *483*, 198.
- [80] A. Mahmood, T. Akram, E. B. de Lima, *J. Mol. Struct.* **2016**, *1108*, 496.
- [81] Ö. Tamer, *J. Mol. Struct.* **2017**, *1144*, 370.
- [82] Ö. Tamer, S. A. Tamer, Ö. İdil, D. Avci, H. Vural, Y. Atalay, *J. Mol. Struct.* **2018**, *1152*, 399.
- [83] Ö. Tamer, D. Avci, E. Çelikoğlu, Ö. İdil, Y. Atalay, *Appl. Organomet. Chem.* **2018**, *32*, e4540.
- [84] P. N. Prasad, D. J. Williams, *Introduction to nonlinear optical effects in molecules and polymers*, Wiley, New York **1991**.
- [85] N. Okulik, A. H. Jubert, *Internet Electron. J. Mol. Des.* **2005**, *4*, 17.
- [86] S. Muthu, A. Prabhakaran, *Spectrochim. Acta. A Mol. Biomol. Spectrosc.* **2014**, *129*, 184.
- [87] E. Scrocco, J. Tomasi, *Adv. Quantum Chem.* **1978**, *11*, 115.
- [88] F. J. Luque, J. M. López, M. Orozco, *Theoretical Chemistry Accounts*, **2000**, *103*(3-4), 343.
- [89] J. S. Murray, K. Sen, *Molecular electrostatic potentials: concepts and applications*, Elsevier, Amsterdam **1996**.
- [90] G. Mahalakshmi, V. Balachandran, *Spectrochim. Acta. A Mol. Biomol. Spectrosc.* **2015**, *135*, 321.

SUPPORTING INFORMATION

Additional supporting information may be found online in the Supporting Information section at the end of the article.

How to cite this article: Rafiq M, Khalid M, Tahir MN, et al. Synthesis, XRD, spectral (IR, UV-Vis, NMR) characterization and quantum chemical exploration of benzoimidazole-based hydrazones: A synergistic experimental-computational analysis. *Appl Organometal Chem.* 2019;e5182. <https://doi.org/10.1002/aoc.5182>